https://ntrs.nasa.gov/search.jsp?R=20190032427 2020-03-10T21:23:41+00:00Z

AGU100 ADVANCING EARTH AND SPACE SCIENCE

Earth's Future

RESEARCH ARTICLE
10.1029/2018EF001123

Key Points:
- Future climate change will increase terrestrial carbon stocks, while future land use change will decrease terrestrial carbon stocks
- Future climate change and land use change will also affect a range of ecosystem functions beyond carbon storage
- However, future changes in ecosystem functioning can often not be explained by future climate change and future land use change alone

Supporting Information:
- Supporting Information S1

Correspondence to:
A. Krause,
andy.krause@tum.de

Citation:
Krause, A., Haverd, V., Poulter, B., Anthoni, P., Quesada, B., Rammig, A., & Arneth, A. (2019). Multimodel analysis of future land use and climate change impacts on ecosystem functioning. *Earth's Future*, *7*, 833–851. https://doi.org/10.1029/2018EF001123

Received 6 DEC 2018
Accepted 6 JUL 2019
Accepted article online 12 JUL 2019
Published online 31 JUL 2019

©2019. The Authors.
This is an open access article under the terms of the Creative Commons Attribution-NonCommercial-NoDerivs License, which permits use and distribution in any medium, provided the original work is properly cited, the use is non-commercial and no modifications or adaptations are made.

Multimodel Analysis of Future Land Use and Climate Change Impacts on Ecosystem Functioning

A. Krause[1,2], V. Haverd[3], B. Poulter[4], P. Anthoni[1], B. Quesada[1,5], A. Rammig[2], and A. Arneth[1]

[1]Institute of Meteorology and Climate Research, Atmospheric Environmental Research, Karlsruhe Institute of Technology, Garmisch-Partenkirchen, Germany, [2]TUM School of Life Sciences Weihenstephan, Technical University of Munich, Freising, Germany, [3]CSIRO Oceans and Atmosphere, Canberra, ACT, Australia, [4]Biospheric Sciences Laboratory, NASA GSFC, Greenbelt, MD, USA, [5]Faculty of Natural Sciences and Mathematics, "Interactions Climate-Environment (ICE)" Research Group, Universidad del Rosario, Bogotá, Colombia

Abstract Land use and climate changes both affect terrestrial ecosystems. Here, we used three combinations of Shared Socioeconomic Pathways and Representative Concentration Pathways (SSP1xRCP26, SSP3xRCP60, and SSP5xRCP85) as input to three dynamic global vegetation models to assess the impacts and associated uncertainty on several ecosystem functions: terrestrial carbon storage and fluxes, evapotranspiration, surface albedo, and runoff. We also performed sensitivity simulations in which we kept either land use or climate (including atmospheric CO_2) constant from year 2015 on to calculate the isolated land use versus climate effects. By the 2080–2099 period, carbon storage increases by up to 87 ± 47 Gt (SSP1xRCP26) compared to present day, with large spatial variance across scenarios and models. Most of the carbon uptake is attributed to drivers beyond future land use and climate change, particularly the lagged effects of historic environmental changes. Future climate change typically increases carbon stocks in vegetation but not soils, while future land use change causes carbon losses, even for net agricultural abandonment (SSP1xRCP26). Evapotranspiration changes are highly variable across scenarios, and models do not agree on the magnitude or even sign of change of the individual effects. A calculated decrease in January and July surface albedo (up to -0.021 ± 0.007 and -0.004 ± 0.004 for SSP5xRCP85) and increase in runoff ($+67 \pm 6$ mm/year) is largely driven by climate change. Overall, our results show that future land use and climate change will both have substantial impacts on ecosystem functioning. However, future changes can often not be fully explained by these two drivers and legacy effects have to be considered.

1. Introduction

Climate change (CC) within the 21st century will have large impacts on terrestrial ecosystems. On the one hand, higher atmospheric carbon dioxide (CO_2) concentrations and longer growing seasons in high latitudes are expected to enhance vegetation growth (e.g., Friend et al., 2014; Zhu et al., 2016). On the other hand, decreasing water availability, more intense heatwaves and droughts, and more frequent disturbances could increase plant mortality (e.g., Seidl et al., 2017). Such changes in vegetation cover may enhance CC via biogeochemical and biophysical feedbacks.

At the same time, terrestrial ecosystems will also be affected by future land use change (LUC; Heck et al., 2018; Krause et al., 2017; Ostberg et al., 2018). Until today, more than two thirds of the ice-free land surface have been modified by some form of human activities like crop cultivation, grazing, or wood harvest (Ellis & Ramankutty, 2008; Klein Goldewijk et al., 2017). Possible future LUC scenarios range from continued deforestation to forest expansion (Hurtt et al., 2011; Popp et al., 2017), depending on a wide range of assumptions including population growth, diet shifts, yield changes, the necessity and type of land-based CC mitigation, and the valuation of the manifold synergies and trade-offs between services associated with different forms of land use (e.g., Alexander et al., 2016; Doelman et al., 2018; Fuss et al., 2018; Krause et al., 2017).

Several modeling studies have investigated the relative importance of historic or future LUC versus CC impacts on ecosystems by studying the effects on variables like vegetation cover and/or carbon cycling globally (e.g., Davies-Barnard et al., 2015; Devaraju et al., 2016; Levy et al., 2004; McGuire et al., 2001; Müller et al., 2007; Ostberg et al., 2015; Tharammal et al., 2018) or regionally (Aleman et al., 2016; Boit et al., 2016; Zaehle et al., 2007; Zhang et al., 2015). However, these studies were often restricted by the usage of only

one model, an inadequate representation of LUC in this model, and/or the focus on one specific variable only. Here, we investigated the isolated and combined global impacts of future CC (including increasing atmospheric CO_2 concentration) and LUC on a range of terrestrial ecosystem functions that are indicative for a number of ecosystem services relevant for climate feedbacks and water cycling: total carbon storage and fluxes, total annual evapotranspiration, January and July surface albedo, and total annual runoff. We ran three dynamic global vegetation models (DGVMs) with input from three combinations of future CC and LUC projections, thereby accounting for model structural uncertainties and covering a range of possible scenarios. We analyzed changes in ecosystem function between present day (2006–2025 average) and the end of the 21st century (2080–2099 average) and used sensitivity simulations to determine the individual contributions of future CC and LUC. We thus went beyond existing studies by (1) using common up-to-date, spatially explicit LUC scenarios (including gross transitions arising from shifting cultivation, as well as wood harvest) from version 2 of the Land Use Harmonization (LUH2) data set (http://luh.umd.edu/); (2) using a multimodel approach including—at least in some of the applied DGVMs—an explicit representation of forest age structure and regrowth, a detailed representation of land management, and an integrated nitrogen cycle; (3) performing transient simulations as well as simulations with either fixed CC or fixed LUC, allowing for the calculation of the total effect as well as the isolated future CC and LUC effects and residual changes not explained by these two drivers; and (4) analyzing a larger range of ecosystem functions beyond carbon storage within three consistent modeling frameworks.

With our study, we particularly aimed to contribute to international policy agreements, especially for land-based mitigation policies, in view of identifying carbon uptake potentials and trade-offs and cobenefits with ecosystem functions beyond carbon storage.

2. Materials and Methods

2.1. Land Use and CC Scenarios

We used three combinations of LUC scenarios (based on Shared Socioeconomic Pathways, SSPs) from the recently released LUH2 data set and corresponding climate projections (Representative Concentration Pathways, RCPs) from the IPSL-CM5A-LR climate model (Dufresne et al., 2013). These climate projections were performed and bias corrected for CMIP5/ISI-MIP2a using observations from ERA-40 (daily) and CRU TS2.1 (monthly) for the reference period 1960–1999 and preserving absolute changes in monthly temperature and relative changes in monthly precipitation (Hempel et al., 2013). The SSPs describe future changes in the energy mix, technological progress, population growth, diets, and global collaboration, while the RCPs are the outcomes of climate policies. Ambitious mitigation goals like the 2 °C target (RCP2.6) can often not be achieved by Integrated Assessment Models under the assumption of regional rivalry and high population growth (like SSP3). Due to the large computational demand of our simulations, we chose only three combinations of SSPs and RCPs reflecting a range of future LUC and CC scenarios. We chose climate projections from IPSL-CM5A-LR because simulated temperature and precipitation changes are quite representative for the ISI-MIP ensemble mean (Warszawski et al., 2014) and because computational limitations did not allow for the consideration of additional climate models. For one of the SSPs (SSP3), the LUC marker scenario from LUH2 is actually associated with an increase in radiative forcing of 7.0 W/m2 (SSP3xRCP70). However, since no ISI-MIP2a IPSL_CM5A-LR RCP7.0 climate was available when performing the simulations, we used the IPSL-CM5A-LR RCP6.0 climate projection instead. While LUC and CC projections were thus not exactly consistent, differences between the RCP6.0 and RCP7.0 climate projections were assumed to be relatively small. For simplicity we referred to this combination of LUC and CC scenarios as SSP3xRCP60 within the text.

The combination of SSP1 and RCP2.6 (SSP1xRCP26), realized with the IMAGE Integrated Assessment Model (van Vuuren et al., 2017), represents a sustainable future scenario. It results in substantial agricultural abandonment and consequently net global forest cover expansion starting already in the first half of the century (Figure 1 and Figure S1 in the supporting information) as a result of low population growth, shifts toward less meat-based diets, food waste reductions, and crop yield increases. Typically, pastures are abandoned (−568 Mha), while croplands expand (+251 Mha) due to large-scale cultivation of second-generation biofuels, resulting in a net agricultural abandonment of 317 Mha between 2006–2025 and 2080–2099. Much of this abandoned land is located in China, but natural vegetation expands also in parts of Africa, Europe,

10.1029/2018EF001123

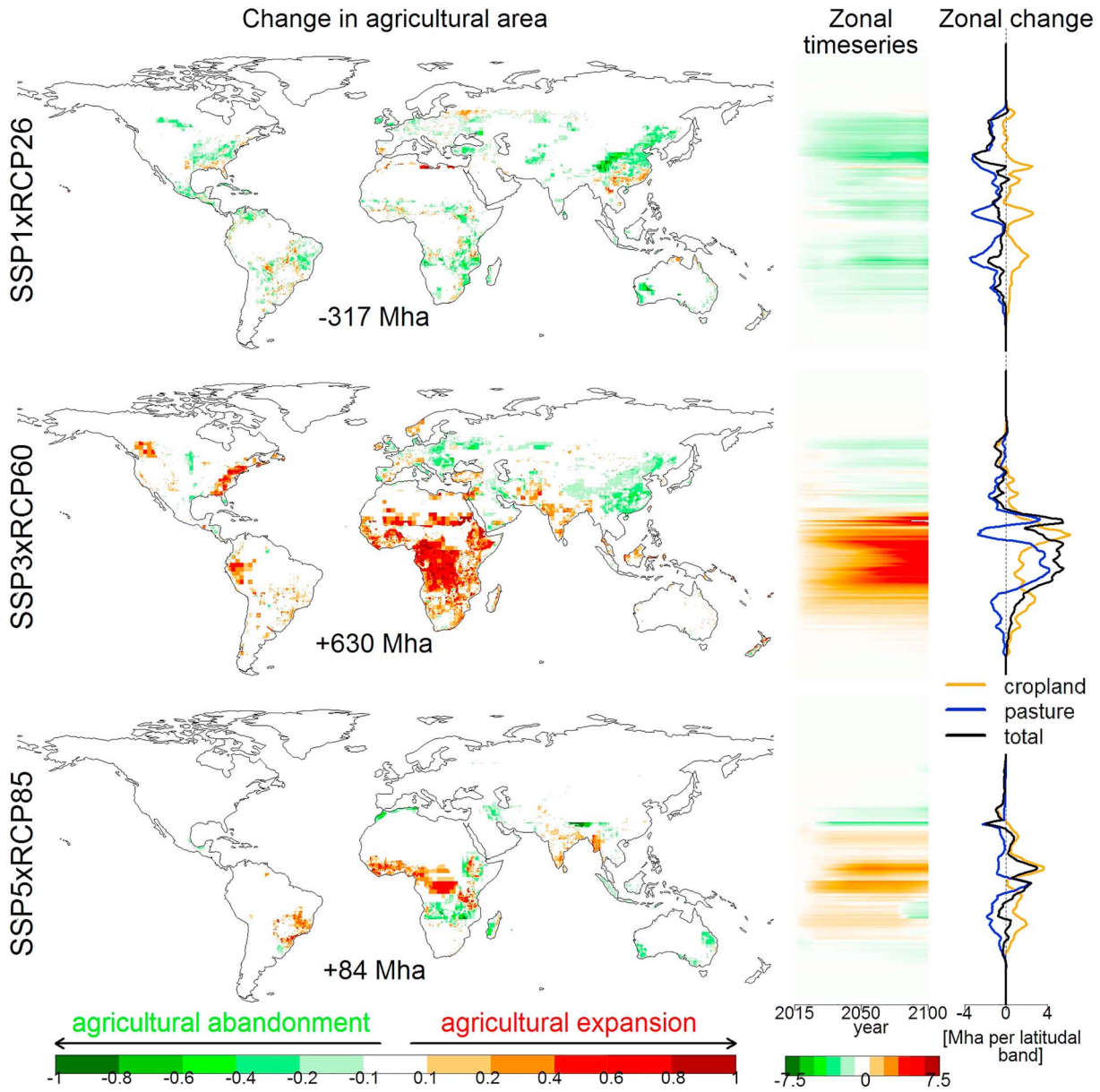

Figure 1. Change in agricultural (cropland plus pasture) fraction between 2006–2025 and 2080–2099 in the three scenarios (left column); zonal time series of agricultural area changes from 2015 to 2100 (middle column); zonal area changes (2.25° running mean) between 2006–2025 and 2080–2090 for croplands (purple), pastures (blue), and croplands plus pasture (black; right column). Values indicated in the bottom-center of the maps are global totals.

North and South America, and Australia (Figure 1). Wood harvest rates increase in parts of Northern Eurasia and Amazonia but decrease at other locations like the southeastern United States (Figure S2). Mean surface air temperature over land as simulated by IPSL-CM5A-LR for RCP2.6 stabilizes at around +0.7 °C compared to the 2006–2025 period (Figure 2), thereby staying below the 2 °C target of the Paris agreement and possibly below its 1.5 °C target. Most tropical and temperate locations are characterized by temperature increases below 1 °C relative to 2006–2025. Precipitation increases in the eastern United States, southern Europe, East Africa, and most of Indonesia but decreases in Australia, South Africa, and most of South America. Atmospheric CO_2 peaks at 443 ppm in the middle of the century and thereafter declines to 421 ppm by the end of the century.

The SSP3xRCP60 scenario, developed by the AIM Integrated Assessment Model (Fujimori et al., 2017), is characterized by large-scale tropical deforestation. Forest cover declines mainly in Africa, while there is

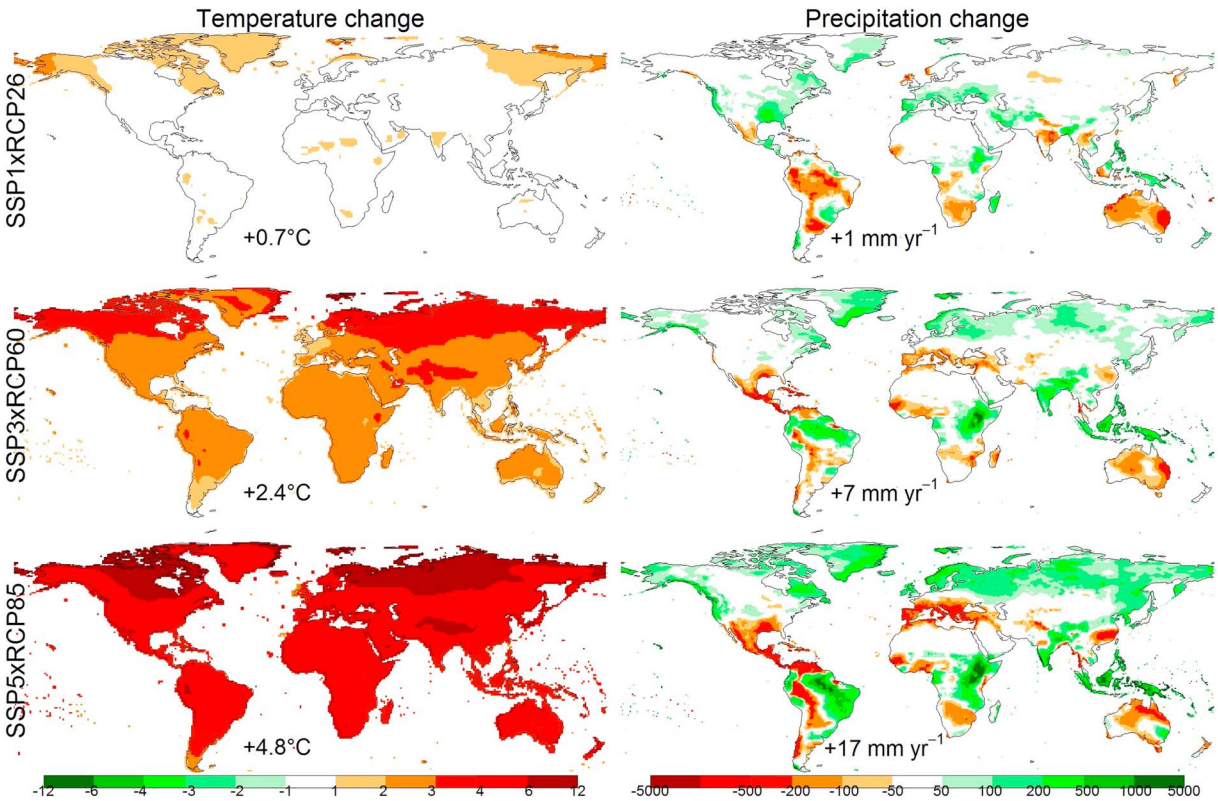

Figure 2. Change in surface annual mean temperature (°C; left column) and mean annual precipitation (mm/year; right column) between 2006–2025 and 2080–2099 in the three scenarios, as simulated by the Earth System Model IPSL-CM5A-LR bias corrected for ISI-MIP2a (Hempel et al., 2013). Values indicated in the bottom-center of the panels are spatial averages over land.

agricultural abandonment in parts of Europe and Asia. Both cropland (+507 Mha) and grazing (+123 Mha) area increases between 2006–2025 and 2080–2099, even though the cultivation of second-generation biofuels is absent in this scenario. The main reasons for this extensification are large population increases, slow yield growth rates, and low intensification of the livestock sector. Agricultural expansion starts in the 2020s and continues throughout the entire century. Changes in wood harvest are similar to SSP1xRCP26, apart from large increases in central and southern Africa and India. The simulated RCP6.0 temperature increase in IPSL-CM5A-LR between 2006–2025 and 2080–2099 is around of 2.4 °C, thus missing the Paris targets. Warming is most pronounced in high latitudes but also exceeds 2 °C at most temperate and tropical locations. Precipitation increases over most tropical and boreal regions but decreases in the subtropics. Atmospheric CO_2 increases throughout the century, reaching 670 ppm in year 2100.

The SSP5-RCP85 scenario was calculated by the REMIND-MAgPIE Integrated Assessment Model (Kriegler et al., 2017). LUC in this scenario is characterized by moderate tropical deforestation, mostly in Africa due to a large increase in crop and livestock demand. Agricultural abandonment takes place at some subtropical locations, some of it only occurring in the last two decades of the 21st century. A decline in pasture area (−159 Mha) is exceeded by simultaneous cropland expansion (+243 Mha). The net increase in agricultural land (+84 Mha), however, is much smaller than in SSP3xRCP60 (+630 Mha). Wood harvest rates increase substantially at many locations, but the increase in Africa is often less pronounced than in SSP3xRCP60. Temperatures rise even higher than for SSP3xRCP60 as a result of higher fossil fuel emissions (but lower LUC emissions), and most land areas suffer from a warming of more than 4 °C. Spatial rainfall patterns are similar to SSP3xRCP60, but changes are more pronounced. Atmospheric CO_2 concentration reaches 936 ppm by the end of the century.

2.2. Dynamic Global Vegetation Models

We use the three combinations of LUC and CC scenarios as input to three DGVMs: LPJ-GUESS, LPJ, and CABLE-POP that contributed to the TRENDYv6 model ensemble (Le Quere et al., 2018). LPJ-GUESS and

CABLE-POP are the only models in the ensemble that account for tree demography effects on biomass accumulation and turnover, making them particularly suited for the representation of secondary forest regrowth. The following paragraphs provide a brief description of the DGVMs. An overview of major model features and differences between the DGVMs can be found in Table 1.

LPJ-GUESS is a process-based ecosystem model that simulates global vegetation patterns as a function of climate, atmospheric CO_2, LUC, and nitrogen inputs (Smith et al., 2014). Woody plant functional types are represented as age cohorts competing for space, light, and soil resources. A number of replicate patches (here: 10 for primary vegetation; 2 for secondary vegetation, i.e., abandoned agricultural land) account for landscape heterogeneity within a grid cell, which is induced by stochasticity in some processes related to establishment and mortality. Carbon assimilated via daily photosynthesis is allocated to leaves, sapwood, and fine roots at the end of each year. Disturbances include stochastic patch-destroying events with an average return interval of 100 years and fire, while windthrows, volcanic eruptions, pests, or insect outbreaks are not simulated explicitly (see Table 1). Soil carbon and nitrogen fluxes are calculated based on the CENTURY model (Parton et al., 1993; Parton et al., 2010; Smith et al., 2014). Besides natural vegetation the model also represents pastures and croplands and their management (Lindeskog et al., 2013; Olin et al., 2015). Surface albedo is not a standard model output but is calculated based on fractional plant cover and albedo baseline values from MODIS satellite as described in Krause *et al*. (2017), with the modification that we set winter albedo of tropical evergreen forests to 0.13 and summer albedo to 0.15 (instead of 0.14 year-round). LPJ-GUESS snow depth was not an output variable so we use LPJ snow depth to derive LPJ-GUESS snow cover.

LPJ shares many ecophysiological features with LPJ-GUESS (Sitch et al., 2003) but represents vegetation dynamics using an "area-based" approach and did not simulate nitrogen cycling and wood harvest (see Table 1). Wildfire was simulated only for the forested tiles using the generalized fire model "Glob-FIRM." LUC is implemented by tiling each grid cell to primary and secondary forest, cropland, and pasture and applying the LUH2 transition matrix to simulate deforestation, agricultural abandonment, shifting cultivation, and crop harvest. Surface albedo is calculated the same as in LPJ-GUESS, that is, using the same albedo values and snow cover, with the only difference being variations in fractional plant cover.

CABLE-POP is a land surface model that represents vegetation structural dynamics and includes a nitrogen cycle. CABLE-POP consists of a biophysics core (Haverd et al., 2016; Kowalczyk et al., 2013; Y. P. Wang et al., 2011), the CASA-CNP biogeochemistry module (Y. P. Wang et al., 2010), the POP module for woody demography and disturbance-mediated landscape heterogeneity (Haverd et al., 2013; Haverd et al., 2014), and a module for land use and land management (POPLUC; Haverd et al., 2018). Generic patch-destroying disturbances occur with an average return interval of 100 years. The land use and land cover change module is driven by gross land use transitions and wood harvest area. CABLE-POP represents coordination of C3 photosynthesis, adjusting electron-transport- and Rubisco-limited rates seasonally to be colimiting (Haverd et al., 2018), leading to a higher simulated CO_2 fertilization effect on photosynthesis than LPJ and LPJ-GUESS (the less CO_2-sensitive electron-transport limitation dominates in these models). Simulated albedo is an outcome of canopy radiative transfer, which follows the approach of Goudriaan and Van Laar (1994).

2.3. Simulation Protocol

All simulations started with a spin-up in order to allow the carbon pools to reach equilibrium with the preindustrial climate and CO_2 (see Table 1), followed by a common historic period (1901–2014) with transient LUC (release "LUH2 v2h") and climate/CO_2. Each group used their standard spin-up procedure (Le Quere et al., 2018) to facilitate the experiment setup and to assure comparability with existing simulations. As the IPSL-CM5A-LR climate data were only available from 1950 onward we randomly recycled years from the 1950–1959 period prior to year 1950. The scenarios only diverged for the future period (2015–2099). All three DGVMs performed the same set of transient simulations (SSP1xRCP26, SSP3xRCP60, and SSP5xRCP85). To separate LUC versus CC effects, we ran factorial experiments and conducted two additional simulations per DGVM with either fixed land use or fixed climate (including fixed atmospheric CO_2) from 2015 on. We implemented fixed LUC by simulating no more land cover transitions but continuing wood harvest (in LPJ-GUESS and CABLE) at average 1995–2014 rates. For the fixed climate/CO_2 simulations we repeated 1995–2014 radiation and precipitation and a detrended temperature signal (cyclic cycles in LPJ-GUESS

10.1029/2018EF001123

Table 1
Overview of Settings and the Representation of Various Processes in the Three DGVMs

Variable or process	DGVM		
	LPJ-GUESS	LPJ	CABLE-POP
Input variables	2-m air temperature, precipitation, downwelling shortwave radiation, nitrogen deposition and fertilization, atm. CO_2, LUC, and soil texture (FAO, 1991)	2-m air temperature, precipitation, downwelling shortwave radiation, atm. CO_2, LUC, and soil texture (FAO, 2012)	Minimum and maximum 2-m air temperature, longwave and shortwave downwelling radiation, precipitation, all downscaled to 3-hourly resolution, nitrogen deposition, atm. CO_2, LUC, and soil texture (FAO, 2012)
Spin-up	500 years (1901–1930 climate, 296 ppm CO_2, 1850 land use map)	1,000 years (1901–1920 climate, 296 ppm CO_2, 1860 land use map)	Five repetitions of full model run (1901–1920 climate, 1,500 land cover, CO_2, nitrogen deposition), paired with a semianalytic spin cycle (Xia et al., 2012). Initialization for 1500–1859 with dynamic land use forcing. The full model (actual CO_2 and nitrogen deposition) was then run for the 1860–2016 analysis period for all scenarios, with 1901–1920 meteorology recycled prior to 1901
Spatial resolution	0.5° × 0.5°		1.0° × 1.0°
Nitrogen cycle	Yes	No	Yes
Natural disturbances	Wildfire, stochastic patch-destroying events	Wildfire	Stochastic patch-destroying events
Implementation of land use patterns from LUH2 into the DGVM	Cropland, pasture, and natural vegetation fractions prescribed by LUH2; PFT distribution on natural land is simulated dynamically		Cropland, pasture, and natural vegetation fractions prescribed by LUH2; PFT distribution on natural land is static
Gross transitions		Yes, differentiation between primary and secondary natural vegetation	
Fate of woody biomass after deforestation	80% (transition to pasture) or 97% (transition to cropland) directly oxidized or stored in product pool; remainder goes to litter	50% of sapwood and 100% of heartwood directly oxidized and returned to atmosphere (no product pool)	Harvested and cleared biomass that is not left as residue is extracted into three product pools. Fractions of harvested and cleared biomass that remain in the landscape as litter are prescribed following Hansis *et al.* (2015)
Wood harvest	Yes (clear-cut, harvested area from LUH2, carbon densities simulated by LPJ-GUESS, 66% of woody biomass removed; remainder to litter)	No	Yes (a secondary harvest event sequentially depletes the areas of each age class, starting from the oldest, until all harvest area is satisfied, subject to land availability)
Dynamic vegetation	Yes		Structural dynamics but not biome shifts

10.1029/2018EF001123

Table 1
(continued)

Variable or process	DGVM		
	LPJ-GUESS	LPJ	CABLE-POP
Number of natural PFTs	12 (10 trees, C3 and C4 grass)	9 (7 trees, C3 and C4 grass)	7 (5 woody PFTs, C3 and C4 grass)
Forest (re)growth dynamics	Cohort approach (competition between different age classes)	Area-based approach (mean individual)	Cohort approach (competition between different age classes)
Implementation of agricultural expansion		All natural PFTs are reduced proportionally	
Representation of pastures	Competing C3 and C4 grass, grazing (50% of ag biomass removed), no trees	Competing C3 and C4 grass, grazing (100% of biomass returned to the litter), no trees	C3 or C4 grassland, grazing (50% of ag biomass removed), no trees
Representation of croplands	LUH2 crop types grown as C3 (wheat) or C4 (maize) cereals, harvest (90% of grain, 75% of residuals), variable sowing and harvest date, tillage, irrigation, fertilization, dynamic potential heat unit calculation, cover grass between growing period (only for perennial crops), no trees	Same as pastures	C3 or C4 cropland with increased soil carbon turnover by tillage, harvest (90% of ag biomass), no trees

Note. DGVM = dynamic vegetation model; LUH = Land Use Harmonization; PFT = plant functional type; FAO = Food and Agriculture Organization.

and LPJ and randomly selected years in CABLE-POP) and kept CO_2 at year 2014 levels. Additional required input variables (e.g., soil maps) were left to the responsibility of the individual DGVM groups. The total effect of all environmental changes on ecosystem functions was then calculated as the change in the transient simulation between the 2006–2025 period and the 2080–2099 period, while the isolated CC and LUC effects were calculated as the 2080-2099 values in the transient simulation minus the 2080–2099 values in the fixed climate and fixed land use simulation, respectively. The residual effect (changes not explained by future CC and LUC) was calculated as the total effect minus the sum of the CC effect and the LUC effect.

3. Results

3.1. Changes in Total Carbon Pools Due to Land Use and CC

Present-day simulated carbon pools and fluxes are in relatively good agreement to other studies (Table S1). In all scenarios and all DGVMs, total terrestrial carbon (vegetation plus soil, including litter, excluding harvested carbon that is stored in product pools) increases between the beginning (2006–2025) and the end (2080–2099) of the century (red circles in Figure 3a), despite the very different CC and LUC projections. Model agreement in terms of total carbon uptake is relatively high for the large-scale deforestation/middle-high warming scenario SSP3xRCP60 (45–69 Gt C), but models differ regarding the relative contributions of future CC and LUC (colored bars in Figure 3). LPJ simulates a much smaller carbon loss due to LUC (−81 Gt C) than LPJ-GUESS (−155 Gt C) and CABLE-POP (−215 Gt C), which is balanced by smaller positive contributions from CC (+55 versus +56 and +103 Gt C). The residual effect (+95 versus +144 and +180 Gt C), calculated as the difference between the carbon uptake in the transient simulations and the sum of the separately simulated CC (plus CO_2) and LUC effects, increases total carbon substantially in SSP3xRCP60 for all three DGVMs. These features also emerge in SSP1xRCP26 and SSP5xRCP85, but in these cases total carbon uptake in the transient LPJ simulations is substantially lower than in LPJ-GUESS and CABLE-POP.

The effect of future CC (including atmospheric CO_2 concentration and including direct effects such as biome shifts as well as indirect effects, e.g., via changes in fire activity due to changing fuel moisture and availability) on total carbon storage varies across scenarios (orange bars in Figure 3a): In SSP1xRCP26 the values range from a very small uptake (LPJ-GUESS) to a small loss (LPJ). CC in SSP3xRCP60 always results in a substantial carbon uptake, especially for CABLE-POP. SSP5xRCP85 leads to a carbon gain for LPJ-GUESS and CABLE-POP but a small carbon loss for LPJ. These differences are explained in part by the differing CO_2 fertilization effect on gross primary productivity (Figure S3) and thereby carbon

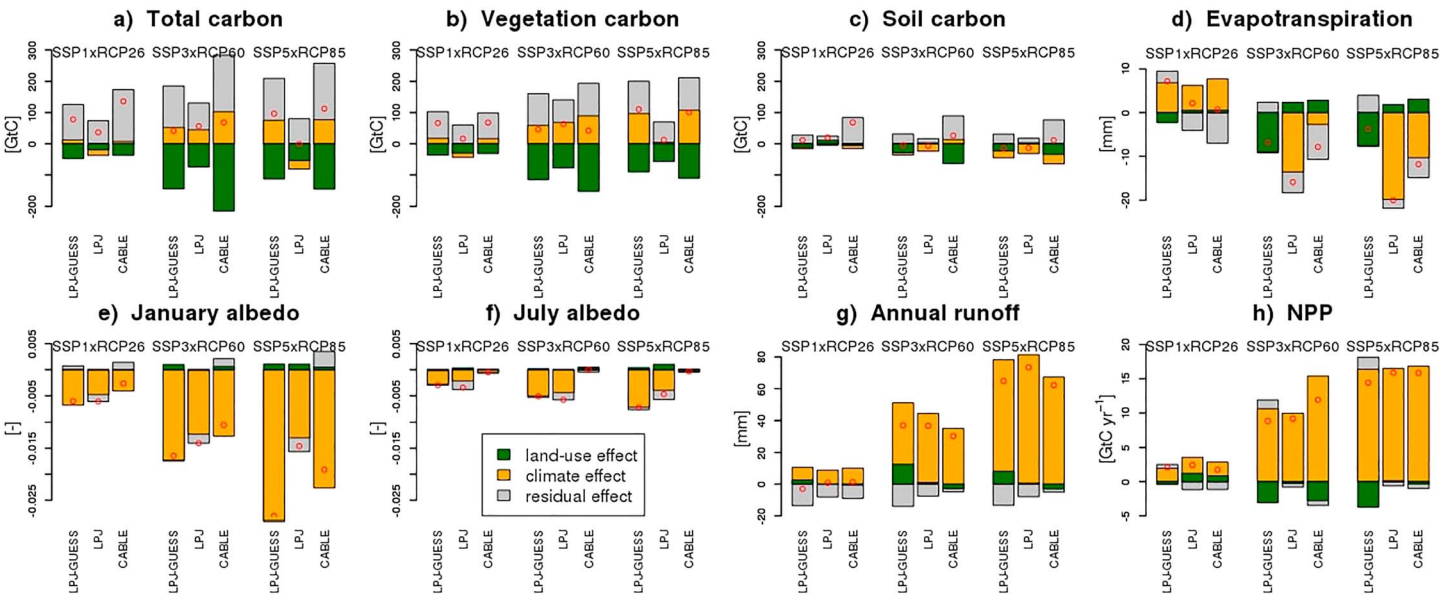

Figure 3. Global change (2006–2025 to 2080–2090) in the transient simulations (red circles) and the individual contributions of land use change (green bars), climate change (orange), and the residual effect (change in the transient simulations minus the sum of the land use and climate effects; gray), for total carbon (Gt C; a), vegetation carbon (Gt C; b), soil carbon (including litter; Gt C; c), total evapotranspiration (mm/year; d), January surface albedo (−; e), July surface albedo (−; f), total runoff (mm/year; g), and net primary productivity (NPP; Gt C/year; h).

storage among the three DGVMs, which is highest for CABLE-POP and lowest for LPJ. However, the CC effect on net primary productivity seems to be comparable in the models, at least for SSP5xRCP85 (Figure 3h). Most of the CC-induced increases in total carbon can be attributed to the vegetation response to CC (Figure 3b), while the effect of CC on global soil carbon (Figure 3c) is either zero or a small carbon loss. Spatially, changes in total carbon in response to CC are found in both low and high latitudes but there is little agreement on the sign of change across the DGVMs (Figures 4 and S4). Spatial changes in vegetation carbon (Figure S5) look similar to spatial changes in total carbon, while soil carbon patterns are quite different (Figure S6). The most prominent feature is a large-scale vegetation carbon loss in the

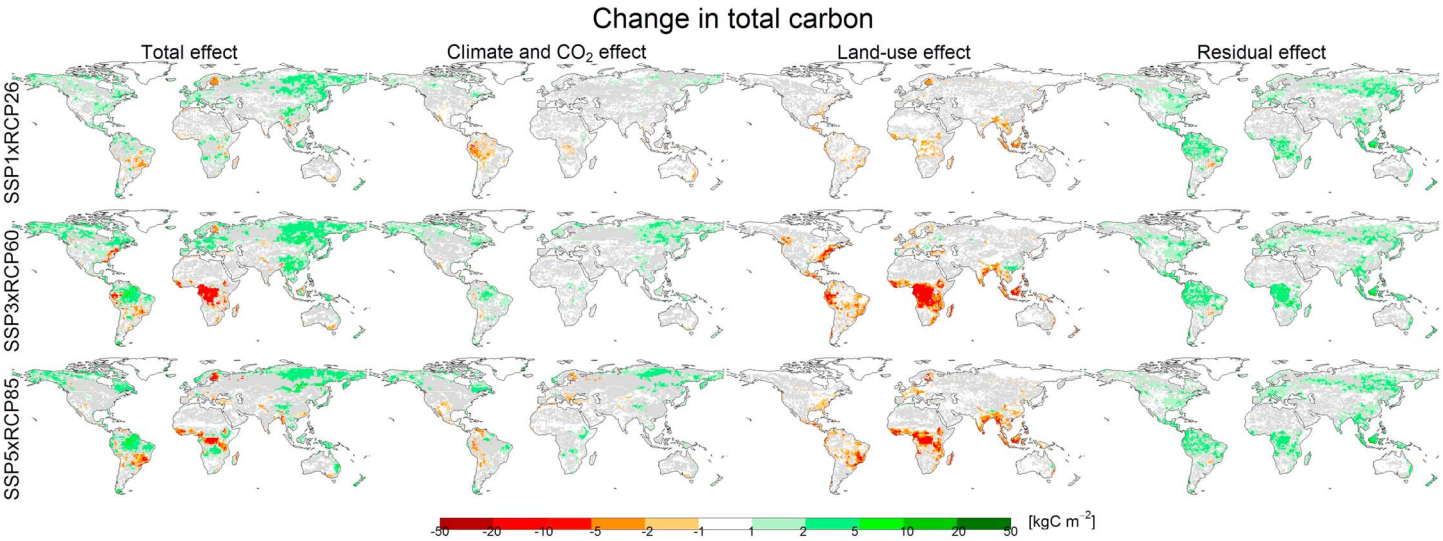

Figure 4. Maps of changes (2006–2025 to 2080–2099) in total carbon pools for the three scenarios averaged over the three DGVMs (different rows), for the total effect (first column), climate effect (second column), land use effect (third column), and residual effect (fourth column). Regions where the DGVMs do not agree on the sign of change are masked in gray. Maps for the individual DGVMs can be found in Figure S4. DGVM = dynamic vegetation model.

boreal zone in LPJ, especially for SSP5xRCP85. This is due to a simulated dieback of boreal forests (Figure S7) at the benefit of herbaceous vegetation (Figure S8), which for the land management version of LPJ has in previous studies been attributed to increased tree mortality due to heat and water stress (Friend et al., 2014; Ostberg et al., 2018).

Future LUC always decreases total carbon pools (green bars in Figure 3a), even in the SSP1xRCP26 scenario in which net agricultural abandonment (pastures plus croplands) takes place (see Figures 1 and S1). We attribute this somewhat surprising outcome in SSP1xRCP26 to a combination of several factors: unsuitable conditions for forest regrowth at locations where agricultural land is abandoned; slow biomass accumulation in regrowing forests (compared to the instant deforestation flux, which still occurs in the transient simulations); calculation of the LUC effect by comparing the transient simulation to a simulation in which gross transitions were stopped from year 2014 on (resulting in carbon uptake as the young forests are not converted to agriculture any more); large-scale pasture abandonment but cropland expansion (croplands substantially deplete soil carbon stocks while pastures can sometimes increase soil carbon; see, e.g., Guo & Gifford, 2002); and increasing wood harvest at some locations (see Figure S2). The substantial differences across DGVMs with respect to the magnitude of the LUC effect can be partly explained by LPJ simulating neither wood harvest (so if harvest rates increase in the future like in SSP3xRCP60 and SSP5xRCP85 the carbon loss from LUC would be underestimated) nor specific crop functional types (see Arneth et al., 2017; Pugh et al., 2015), and by large differences in simulated present-day vegetation (336, 520, and 431 Gt C for LPJ-GUESS, LPJ, and CABLE, respectively) and soil (1,463, 1,384, and 1,518 Gt C) carbon pools (see also W. Li et al., 2017).

In most cases total future carbon uptake in the transient simulations is much larger than the sum of the isolated CC and LUC effects (this difference is represented by the gray bars in Figure 3); that is, ecosystems are simulated to take up additional carbon even if both CC and LUC and were kept constant from now on. The main reason is that ecosystems are not yet in equilibrium with present-day land use (e.g., forest regrowth and soil carbon accumulation after agricultural abandonment takes decades or even centuries; see, e.g., Krause et al., 2016), climate (tree growth in high latitudes), and/or atmospheric CO_2 (enhanced forest productivity due to CO_2 fertilization). In addition, changes in other environmental drivers (e.g., nitrogen deposition in LPJ-GUESS and CABLE-POP; see Figure S9) also impact ecosystem carbon storage. However, additional sensitivity experiments with LPJ-GUESS as well as earlier studies (Tharammal et al., 2018; Warlind et al., 2014) suggest that this effect is relatively small. Lastly, at some locations synergies between future CC and LUC might not be captured by the sum of the isolated CC and LUC effect. For example, in the transient simulations natural vegetation expansion on former agricultural fields might result in biomass accumulation because CC favors forest regrowth on these abandoned agricultural lands, while the sum of the isolated LUC effect—no change in carbon pools because tree growth is not allowed in agricultural areas—and the isolated CC effect—no change because present-day climate conditions might not favor tree growth at these locations—might be 0, resulting in a calculated carbon uptake via the residual effect.

3.2. Changes in Evapotranspiration

Despite the same forcings used in all DGVMs, total terrestrial evapotranspiration changes in the transient simulations are highly variable across DGVMs (Figure 3d). Evapotranspiration increases in SSP1xRCP26, especially for LPJ-GUESS, but decreases for SSP3xRCP60 and SSP5xRCP85, especially for LPJ. Increases are generally found in high latitudes, whereas evapotranspiration is found to decrease in the tropics and subtropics, particularly for SSP3xRCP60 and SSP5xRCP85 (Figure 5). The CC, LUC, and residual effect all play an important role to explain the substantial spatial differences between DGVMs, for example, the large evapotranspiration decrease in LPJ-GUESS over central Africa for SSP3xRCP60 contrasting the large increase in CABLE-POP (Figure S10).

In all DGVMs, future CC causes a net global evapotranspiration increase in SSP1xRCP26, with spatial patterns (Figure 5) roughly following precipitation changes (Figure 2). In SSP3xRCP60 and SSP5xRCP85, however, the global CC effect ranges from virtually zero (LPJ-GUESS) to a substantial decrease (LPJ), despite globally increasing temperatures and rainfall. We interpret this to be a result of different effects of increasing atmospheric CO_2 on plants' water use efficiency and productivity in the DGVMs. For the SSP5xRCP85 scenario, average water use efficiency (annual gross primary productivity/evapotranspiration) increases by the end of the century by 0.67 g C/kg H_2O in LPJ-GUESS, by 0.83 g C/kg H_2O in LPJ, and by 0.76 g C/kg H_2O in

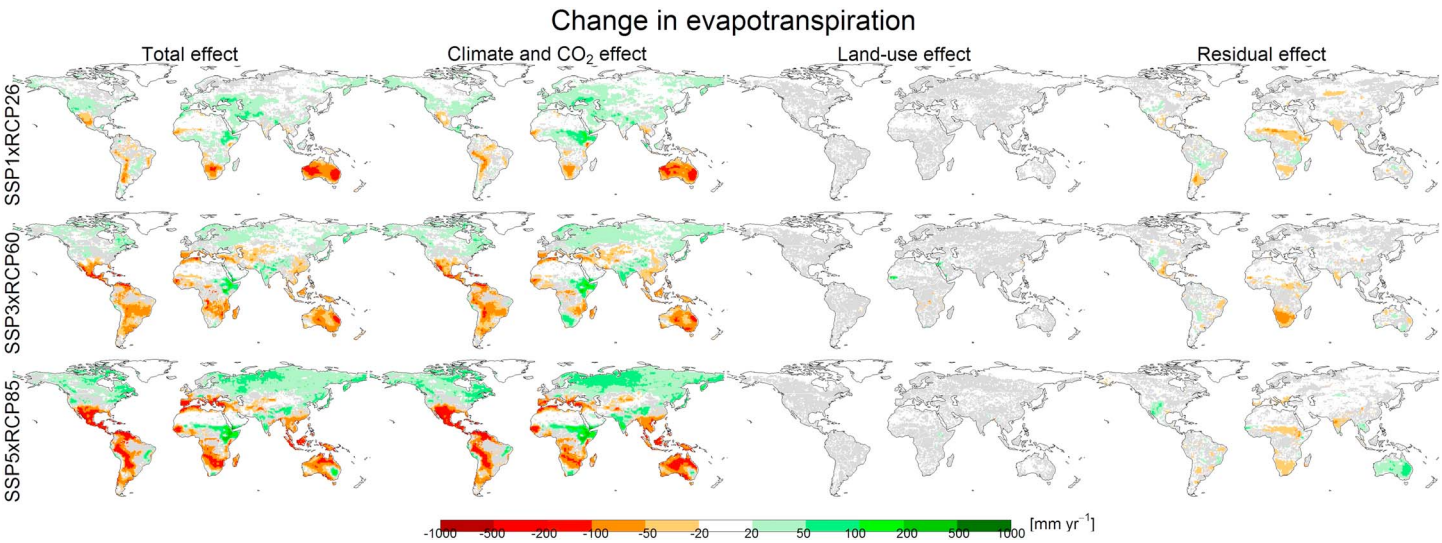

Figure 5. Same as Figure 4 but for evapotranspiration.

CABLE. Regionally, evapotranspiration over Brazil in SSP5xRCP85 can increase (LPJ-GUESS), decrease (LPJ), or increase/decrease, depending on location (CABLE-POP). In high latitudes, evapotranspiration increases more for LPJ-GUESS than for LPJ and CABLE-POP. Presumably, this occurs because tropical and boreal trees grow less leaves or use water more efficiently in LPJ and CABLE-POP relative to LPJ-GUESS under higher CO_2 concentrations.

In all scenarios, LUC results in substantial evapotranspiration decreases for LPJ-GUESS but increases for LPJ and CABLE-POP. These differences are most apparent for the tropical deforestation cases SSP3xRCP60 and SSP5xRCP85 (Figures 1 and S10). The evapotranspiration increase in LPJ and CABLE-POP in response to deforestation is quite surprising, given that forests typically transpire more water than other land cover classes (see discussion). LPJ and CABLE-POP simulate a strong decline in transpiration response to deforestation in energy-limited regions like central Africa (SSP3xRCP60), but this is accompanied by a larger simulated increase in soil evaporation facilitated by higher radiation absorption by the ground and less resistance to evaporation by litter.

The residual effect increases global evapotranspiration in LPJ-GUESS but decreases it in LPJ and CABLE-POP, thereby counteracting the LUC effect. These differences between models are hard to interpret, especially since there are also regions where the models agree on the sign of change, for example reductions in the Sahel, southern Africa, India, and some temperate regions. For SSP5xRCP85 the residual effect increases evapotranspiration in Australia and the southwestern United States in all DGVMs. In LPJ-GUESS, however, unlike in the other DGVMs, there is a large increase in central Africa and southeastern Asia.

3.3. Changes in Surface Albedo

The decrease in global land surface albedo is generally more pronounced in the high-warming scenarios. Albedo decreases mostly in January (Figure 3e), but despite a much smaller reduction in seasonal snow cover (Figure S11), we also find substantial albedo decreases in July (apart from CABLE-POP, Figure 3f). The LPJ-GUESS SSP1xRCP26 January albedo reduction is slightly smaller than the decrease in the baseline LUC scenarios of Krause *et al*. (2017) where snow depth was taken from LPJ-GUESS. In all scenarios, the albedo reduction is largely concentrated in middle and high latitudes, that is, for January in the temperate and boreal zone (Figure 6) or for July even further north in arctic regions (Figures 7). However, there are also large areas in North America and Central Russia (LPJ) or Eastern Russia (CABLE-POP) where albedo increases substantially, particularly in January (Figures S12 and S13). The total effect is dominated by the CC effect, but there is sometimes also a small, counteracting LUC effect and a substantial residual effect.

10.1029/2018EF001123

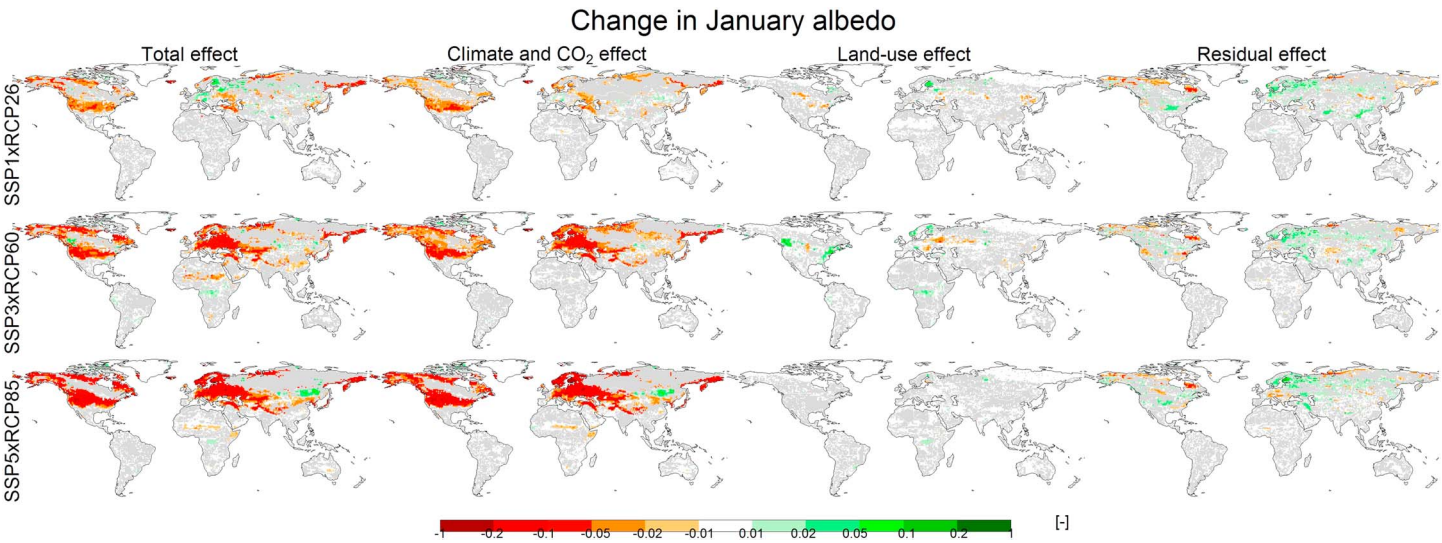

Figure 6. Same as Figure 4 but for January surface albedo.

CC typically causes large reductions in surface albedo. This is often due to the combination of declining snow cover and forest growth in high latitudes. January snow cover in LPJ (and thus also in LPJ-GUESS) shrinks mostly in eastern and northern Europe and Central North America (Figure S12). On average, 26 Mha (1%) and 71 Mha (28%) of snow disappear globally in January, respectively July, for SSP1xRCP26, and 682 Mha (19%) and 210 Mha (78%) for SSP5xRCP85. Interestingly, in LPJ there are regions of substantial January albedo increases neighboring regions of large albedo reductions. These are often locations where the snow does not disappear but grass cover increases at the expense of forests (Figures S7 and S8). In regions further north/south the trees survive or even establish in former tundra, resulting in decreasing surface albedo. Small albedo reductions are also found in the tropics (LPJ-GUESS and LPJ) as a result of more vegetation/tree cover due to CC. In CABLE-POP, vegetation composition does not respond to CC so the increase in surface January albedo found in northeastern Asia has to be chiefly related to increasing snow cover despite surface warming. The global decrease in SSP5xRCP85 January albedo from melting snow, however, is larger in CABLE-POP than in LPJ-GUESS and LPJ when assuming static present-day vegetation cover in LPJ-GUESS and LPJ (0.023 versus 0.016 and 0.015).

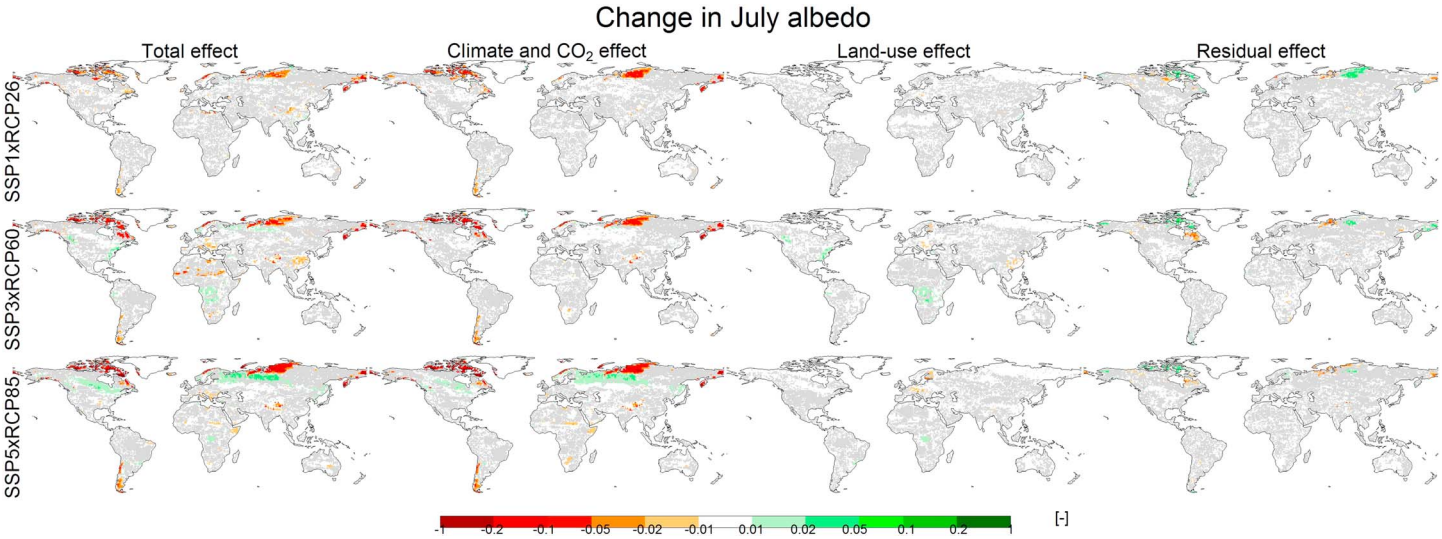

Figure 7. Same as Figure 4 but for July surface albedo.

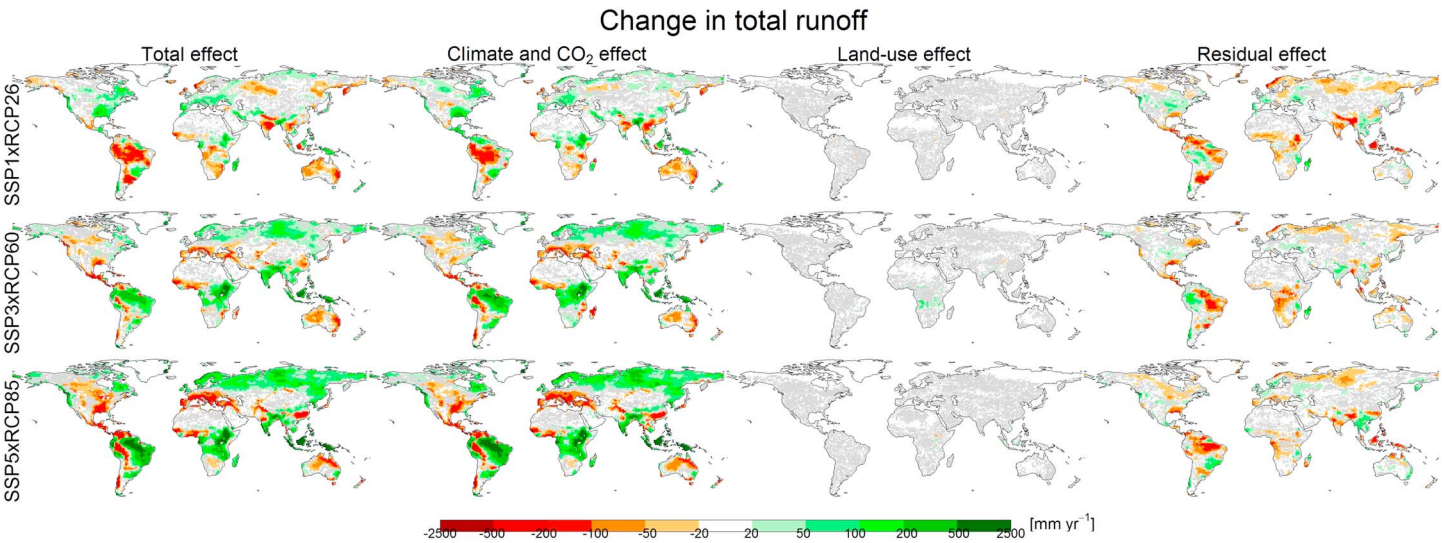

Figure 8. Same as Figure 4 but for total runoff.

Globally, the effect of future LUC is either zero or an increase in surface albedo for all scenarios (Figures 3e and 3f), and there is substantial model agreement at regional scale, at least for LPJ-GUESS and LPJ (Figures S12 and S13). Regional changes reflect changes in vegetation cover (Figures S7 and S8). Interestingly, for LPJ-GUESS and LPJ the SSP3xRCP60 deforestation scenario results in an albedo increase in tropical Africa and some boreal regions (January, presumably partly due to wood harvest; see Figure S2) but a decrease at some subtropical and temperate locations. The latter is due to forest expansion (Figure S7) and also due to LUC-related changes in total vegetation cover (Figure S14). For example, in SSP3xRCP60 bare soils of very high albedo (Figure S15) are increasingly covered by vegetation in northern Africa, while bare soils of low albedo expand in parts of Asia. However, the large LUC-induced increase in simulated vegetation cover seems quite unrealistic in the eastern Sahel/Sahara region where the increase is related to pasture expansion. In the western part, however, the increase is mainly due to expansion of irrigated croplands, which might indeed increase vegetation cover.

The residual effect can be an albedo decrease (LPJ), increase (CABLE-POP January), or zero (LPJ-GUESS January and July; CABLE-POP July). The spatial patterns are heterogeneous and often hard to interpret due to complex interactions between changes in vegetation types, bare soil, and snow cover. In high latitudes, the residual effect often increases total vegetation cover (LPJ-GUESS and partly in LPJ; see Figure S14) but in the boreal zone sometimes reduces forest cover (Figure S7). The most likely explanation is that the repeating 1995–2014 climate cycle used in the fixed climate simulation has too little precipitation in this area to sustain forest growth. This often decreases January albedo in present-day tundra regions but increases albedo in taiga regions. In the tropics, the effect is very small.

3.4. Changes in Runoff

Total annual runoff hardly changes in SSP1xRCP26 but increases by on average more than 30 mm/year in SSP3xRCP60 and more than 60 mm/year in SSP5xRCP85 (Figure 3g). Differences between DGVMs seem less pronounced than for evapotranspiration partly due to the large overall increases. Spatial patterns look similar across all DGVMs (Figures 8 and S16).

Changes in total runoff in the transient simulations are mostly due to CC, especially for the high-warming scenarios. Spatial patterns of the CC effect seem to be largely driven by precipitation changes (Figure 2). Averaged over all grid cells, total runoff increases by 84, 88, and 92 mm (LPJ-GUESS, LPJ, and CABLE-POP) per 100-mm increase in annual precipitation (not shown).

The LUC effect on total runoff is largest for LPJ-GUESS and virtually nonexistent in LPJ. Spatially, changes are typically opposite to LUC-induced evapotranspiration changes, which is not surprising as rainwater has

to leave the system either via evapotranspiration or runoff (neglecting the limited storage capacities of the soil).

The residual effect always leads to a reduction in global mean runoff but in all models and scenarios there are also regions were the residual effect increases runoff. Spatial patterns look similar across DGVMs, for example the reductions found at many high-latitude locations and in equatorial South America.

4. Discussion

In this study, we analyzed changes in a range of ecosystem functions simulated by three DGVMs and for three combinations of future CC and LUC scenarios. For some variables (carbon pools, evapotranspiration, and January albedo) differences across DGVMs in the transient (CC + LUC) simulations can be comparable in magnitude to differences across scenarios. With respect to carbon storage, the positive impacts of moderate CC and CO_2 fertilization are typically offset by negative LUC effects, but the net change in the transient simulations is still a carbon uptake due to a large positive residual effect (i.e., enhanced forest growth mostly due to historic LUC, CC, and CO_2 increases). Albedo reductions and increases in runoff are largely driven by future CC, while future LUC only has small impacts. Evapotranspiration changes show the largest variability across scenarios, and the DGMVs do not agree on the magnitude or even sign of change of the CC effect and the LUC effect.

Several modeling studies previously investigated the combined and isolated effects of future CC and LUC on global terrestrial carbon cycling (Table 2), even though methodologies differed substantially across studies. Levy *et al.* (2004) reported large carbon uptake (2–6 Gt C/year) simulated by the HyLand DGVM for four Intergovernmental Panel on Climate Change Special Report on Emission Scenarios, mostly due to increasing CO_2, with smaller contributions from future CC and LUC, and a small residual effect (not explicitly mentioned). Using the LPJmL DGVM, Müller *et al.* (2007) found a total carbon uptake (~60 Gt C between 2015 and 2090) for the low-warming/afforestation Special Report on Emission Scenarios B1 scenario but a large loss (−115 Gt C) for the high-warming/deforestation A2 scenario. While Müller et al. calculated a CC effect of up to +130 Gt C (note that this includes the residual effect according to their calculation), LUC reduced total carbon by up to 270 Gt C for the A2 scenario (note that deforestation—mainly in South America—was much more pronounced compared to our study, about 1,500-Mha increase in cultivated area, including managed forests but mainly croplands), which is broadly in agreement with the carbon loss from (less) deforestation in our study. Lastly, two recently studies (Davies-Barnard et al., 2015; Tharammal et al., 2018) explored the CC versus LUC effects on total carbon uptake in two Earth System Models (ESMs; HadGEM2-ES and CESM1) for three RCP scenarios. While Davies-Barnard *et al.* (2015) calculated the LUC effect as in our approach, the remaining carbon changes were assigned between "climate-induced land cover changes" and "not from land cover changes." Davies-Barnard and colleagues found that land cover changes resulting from CC are generally more important than LUC. However, the large CC-induced soil carbon uptake in HadGEM2-ES is impugned by isotopic data analysis (Y. J. He et al., 2016). Furthermore, Davies-Barnard *et al.* (2015) simulated a large vegetation carbon uptake in response to afforestation. This may be partly due to the lack of nitrogen limitation in HadGEM2-ES and the less detailed representation of LUC compared to our study (see Arneth et al., 2017). Tharammal *et al.* (2018) found an overall CC effect (including CO_2) of 13–61 Gt C for the same RCPs, and a LUC effect of −93 to +29 Gt C (calculation different from our study: the change between present day and end of the century in a transient LUC simulation). CESM1 includes a nitrogen cycle and wood harvest, but gross transitions and explicit forest regrowth were not represented. Interestingly, Tharammal *et al.* (2018) reported a much smaller residual effect compared to our study. Potential explanations for this mismatch are the explicit calculation of the nitrogen deposition effect (range −11 to 4 Gt C) in Tharammal *et al.* (2018), static vegetation in CESM1, and in particular differences in the calculation of the LUC (and thus the residual) effect.

Satellite-derived evapotranspiration estimates suggest that terrestrial evapotranspiration declines in response to tropical deforestation under present-day conditions (Alkama & Cescatti, 2016; Duveiller, Hooker, & Cescatti, 2018; Y. Li et al., 2015). In our study, however, this pattern is only reproduced by LPJ-GUESS, while LPJ and CABLE-POP simulate evapotranspiration increases. Irrigation might expand in the future and thus promote evapotranspiration from croplands, but as LPJ and CABLE-POP do not represent cropland irrigation this cannot explain the simulated deforestation-driven increase in

Table 2
Overview of Modeling Studies Investigating the Combined and Isolated Effects of Future CC and LUC on the Terrestrial Carbon Cycle

Study	Variables analyzed	Model applied	Effects considered	CC and LUC projections	Reported changes (time period)
Levy *et al.* (2004)	Net Biome Productivity	HyLand (DGVM)	CC (no CO_2) CO_2 LUC Total	HadCM3 CC projections for the SRES scenarios (A1B, A2, B1, and B2), regional LUC from SRES scenarios applied on 1990 land cover map	−1 to −2 Gt C/year +4 to +7 Gt C/year −1 to +2 Gt C/year +2 to +6 Gt C/year +2 to +6 Gt C/year (1990 to 2100)
Müller *et al.* (2007)	Total carbon pools (also vegetation and soil carbon and carbon fluxes)	LPJmL (DGVM)	CC (with CO_2) LUC Total	Downscaled and interpolated CC and LUC projections from IMAGE implementations of SRES storylines (A2, B1, and B2)	+105 to +225 Gt C −120 to −445 Gt C −279 to +33 Gt C (1970 to 2100)
Davies-Barnard *et al.* (2015)	Total carbon (also vegetation and soil carbon)	HadGEM2-ES (ESM)	CC (with CO_2, only for CC-induced land cover changes) LUC Total	CC simulated by HadGEM2-ES according to three RCP scenarios (2.6, 4.5, 8.5), corresponding LUC from LUH	+30 to +110 Gt C −25 to +45 Gt C +180 to +425 Gt C (2006 to 2100)
Tharammal *et al.* (2018)	Total carbon pools (also vegetation and soil carbon and NPP)	CESM1 (ESM)	CC (no CO_2) CO_2 LUC N deposition Residual Total	CC simulated by CESM1 according to three RCP scenarios (2.6, 4.5, and 8.5), corresponding LUC from LUH	−26 to −7 Gt C +20 to +87 Gt C −93 to +29 Gt C −11 to +5 Gt C +0 Gt C −27 to +55 Gt C (2005–2015 to 2090–2099)
Our study	Total carbon (also vegetation and soil carbon)	LPJ-GUESS, LPJ, CABLE (DGVMs)	CC (with CO_2) LUC Residual Total	IPSL-CM5A-LR CC projections for three RCPs (2.6, 6.0, and 8.5), corresponding LUC from LUH2	−27 to +103 Gt C −215 to −20 Gt C +74 to +180 Gt C −1 to +136 Gt C (2006–2025 to 2090–2099)

Note. DGVM = dynamic global vegetation model; LUH = Land Use Harmonization; NPP = net primary productivity; ESM = Earth System Model; LUC = land use change; CC = climate change; SRES = Special Report on Emission Scenarios.

evapotranspiration in these models. The large intermodel differences are in line with recent studies reporting diverging evapotranspiration responses to deforestation in DGVMs and land surface models (Duveiller, Forzieri, et al., 2018; Mao et al., 2015) but in contrast to the quite uniform decrease found in five ESMs (Quesada et al., 2017). Our three DGVMs also strongly disagree on the CC effect on evapotranspiration. As we used the same climate input in all models, this seems to be largely associated with the net CO_2 effect on evapotranspiration. Increasing atmospheric CO_2 concentration on the one hand reduces plant transpiration via increased water use efficiency and reduced stomatal conductance but also promotes vegetation growth and thereby transpiration from a larger leaf area. Mao *et al.* (2015) analyzed multiple land surface model outputs to study the drivers of variability and trend in evapotranspiration over the 1982–2010 period. They found that the increasing trend can largely be explained by CC (chiefly precipitation), while the net CO_2 effect was a small decrease, especially in regions with dense vegetation cover. The evapotranspiration reduction under moderate-to-high CO_2 concentrations scenarios is consistent with other observational and modeling studies (Field et al., 1995; Pan et al., 2015; Porporato et al., 2001), which agree on the predominance of the stomatal conductance reduction.

To our knowledge, the isolated CC versus LUC effects on future land surface albedo have previously not been analyzed simultaneously, but even the literature on CC-induced changes in future snow cover and albedo is surprisingly scarce. CMIP5 models simulate Northern Hemisphere snow area reductions between 1971–2000 and 2071–2100 of ~−5.6 ± 3.2% and −9.7 ± 3.5% in winter and −16.6 ± 13.8% and −25.1 ± 15.5% in summer for RCP2.6 and RCP4.5, respectively (A. H. Wang et al., 2018). This compares to satellite-based

observations of +1.5% since the 1970s or +17 Mha per decade (January) and −54.9% or −72 Mha per decade (July; https://www.ncdc.noaa.gov/snow-and-ice/extent/snow-cover/nhland/7). The LPJ July snow cover reduction (−28% or −71 Mha) for the SSP1xRCP26 scenario in this study is thus relatively large compared to CMIP5 models (but within the CMIP5 model range and small compared to observations), while January reductions (−1% or −26 Mha) seem comparably small (but large compared to the increase observed over the last decades). Possible reasons for the disagreement across models include the comparison of different time periods and the high sensitivity of snow cover to structural distinctions in the applied snow schemes (Qu & Hall, 2014; Roesch, 2006; Thackeray et al., 2018; Z. Wang & Zeng, 2010). Changes in simulated snow cover and assumed snow albedo then contribute to changes in surface albedo (Y. Li et al., 2016), along with CC-induced changes in forest cover and associated albedo values (Q. P. Li et al., 2018; Loranty et al., 2014). Satellite-based observations over the 1981–2010 period suggest that Northern Hemisphere surface albedo declined in July but increased in January, both changes correlated with changes in snow cover (T. He et al., 2014). Over the 2002–2016 period, Q. P. Li *et al.* (2018) reported a decrease in mean annual albedo of 0.0004, with large variability across regions and varying contributions from snow and vegetation changes. With respect to LUC effects on surface albedo, remote sensing observations show a steady increase in the difference in annual surface albedo between forests and open land toward the pole, from around 0.02 in the tropics to 0.06 in temperate regions and 0.12 in the boreal zone, and up to >0.2 in January in high latitudes (Duveiller, Hooker, & Cescatti, 2018; Y. Li et al., 2015). These patterns are related to albedo differences between vegetation types being amplified in the presence of snow cover and have also been simulated qualitatively in climate models under global deforestation experiments (Davin & de Noblet-Ducoudre, 2010; Devaraju et al., 2015). In our simulations, LUC usually occurs only in parts of the grid cell so albedo changes are often naturally smaller. Our DGVMs also capture the latitude dependency of the LUC effect: The simulated LUC impacts on surface albedo are similar in magnitude in low and high latitudes, despite areas undergoing LUC being largely located in the tropics.

Several studies have investigated the drivers of changes in runoff, typically focusing on annual runoff. One exception is a recent study by Kooperman *et al.* (2018) who found that plant-physiological responses to a quadrupled CO_2 concentration are of similar importance for daily runoff extremes in the CESM ESM as radiative-induced precipitation changes. Gedney *et al.* (2006), using the MOSES land surface model, attributed the increase in global annual runoff observed over the twentieth century mainly to stomatal closure in response to increasing CO_2. However, when also accounting for the CO_2 impact on vegetation productivity in the ORCHIDEE DGVM, Piao *et al.* (2007) found CC and LUC to be much more important than the net effect of CO_2, with uncertainty mainly associated with CO_2 effects on vegetation growth and the contribution of agricultural irrigation to runoff changes. Betts *et al.* (2007) reported an increase in continental runoff versus preindustrial levels in response to the physiological effect of doubled CO_2 concentration on plant transpiration. Gerten *et al.* (2008) found a dominating precipitation effect (~80%) in the LPJmL DGVM and only small contributions from temperature, CO_2, LUC, and irrigation. The dominant role of CC versus LUC was also reported for the second half of the century using the CLM (Shi et al., 2011). Our study indicates that the greater importance of CC (including CO_2) versus LUC will also hold in the future for a range of scenarios. Alkama *et al.* (2013) analyzed future runoff changes in CMIP5 models for the RCP8.5 scenario but did not separate driving variables. They found, besides a global increase, positive trends over northern Asia, Scandinavia, North America, and South Asia, a negative trend over South Europe, no trend over Central America, and model disagreement over South America and Africa. These patterns also occur in our study, apart from decreasing (LPJ-GUESS and CABLE-POP) or stable (LPJ) runoff over North America and decreasing runoff over Central America.

5. Conclusions

We ran an intercomparison of dynamic vegetation modeling sensitivity experiments to assess the impacts and associated uncertainty of CC and LUC on several ecosystem functions: terrestrial carbon storage and fluxes, evapotranspiration, surface albedo, and runoff. Some limitations should be kept in mind when interpreting our results. For instance, CC impacts could substantially be altered by using forcing climate from more than one climate model (Müller et al., 2007; Tao et al., 2014). Furthermore, by prescribing the same CO_2 concentrations in the standard and the constant LUC simulations, we do not capture associated CO_2 fertilization effects and carbon-climate feedbacks, which have been shown to substantially impact

vegetation productivity in ESMs (Quesada et al., 2018), with possibly significant effects on carbon pools, surface albedo, and water cycling. Moreover, while surface albedo in the tropics has been simulated to substantially increase with large-scale deforestation, the planetary albedo was hardy affected due to evapotranspiration-cloud feedbacks (Bala et al., 2007), a process we cannot capture in our offline DGVMs. Similarly, by prescribing precipitation, we cannot simulate potential vegetation feedbacks (Ellison et al., 2012). Nevertheless, our simulations still suggest that both future LUC and CC will have large effects on a range of ecosystem functions. Additionally, we show that there are large differences across existing studies in calculating the isolated LUC and CC effects.

Interestingly, in our approach there can be substantial changes not explained by these two drivers ("residual effect"), especially for carbon pools and evapotranspiration. The most likely explanation is that ecosystems are not yet in equilibrium with present-day land use/climate/CO_2, which should be further explored in a follow-up study. We note that previous modeling studies often performed only one set of sensitivity simulations (usually fixed LUC) and consequently erroneously attributed the leftover changes fully to future CC. Vegetation and climate modelers need to be aware that ecosystems may presently not yet be in equilibrium with their environment, thereby interfering with their findings.

Acknowledgments
We thank the two anonymous reviewers and the Editor for their comments on the manuscript. A. K. was funded by the Helmholtz Association through the International Research Group CLUCIE and by the European Commission's Seventh Framework Programme, under Grant Agreement 603542 (LUC4C). B. Q., P. A., and A. A. also acknowledge support from the LUC4C project. V. H. acknowledges support from the Earth Systems and Climate Change Hub, funded by the Australian Government's National Environmental Science Program. Data underlying the analyses is uploaded on the corresponding author's figshare account (https://figshare.com/articles/Krause_et_al_2019_Earth_s_Future/7951181). The authors declare no conflict of interest.

References

Aleman, J. C., Blarquez, O., & Staver, C. A. (2016). Land-use change outweighs projected effects of changing rainfall on tree cover in sub-Saharan Africa. *Global Change Biology*, *22*(9), 3013–3025. https://doi.org/10.1111/gcb.13299

Alexander, P., Brown, C., Arneth, A., Finnigan, J., & Rounsevell, M. D. A. (2016). Human appropriation of land for food: The role of diet. *Global Environmental Change-Human and Policy Dimensions*, *41*, 88–98. https://doi.org/10.1016/j.gloenvcha.2016.09.005

Alkama, R., & Cescatti, A. (2016). Biophysical climate impacts of recent changes in global forest cover. *Science*, *351*(6273), 600–604. https://doi.org/10.1126/science.aac8083

Alkama, R., Marchand, L., Ribes, A., & Decharme, B. (2013). Detection of global runoff changes: Results from observations and CMIP5 experiments. *Hydrology and Earth System Sciences*, *17*(7), 2967–2979. https://doi.org/10.5194/hess-17-2967-2013

Arneth, A., Sitch, S., Pongratz, J., Stocker, B. D., Ciais, P., Poulter, B., et al. (2017). Historical carbon dioxide emissions caused by land-use changes are possibly larger than assumed. *Nature Geoscience*, *10*(2), 79–84. https://doi.org/10.1038/NGEO2882

Bala, G., Caldeira, K., Wickett, M., Phillips, T. J., Lobell, D. B., Delire, C., & Mirin, A. (2007). Combined climate and carbon-cycle effects of large-scale deforestation. *Proceedings of the National Academy of Sciences of the United States of America*, *104*(16), 6550–6555. https://doi.org/10.1073/pnas.0608998104

Betts, R. A., Boucher, O., Collins, M., Cox, P. M., Falloon, P. D., Gedney, N., et al. (2007). Projected increase in continental runoff due to plant responses to increasing carbon dioxide. *Nature*, *448*(7157), 1037–1041. https://doi.org/10.1038/nature06045

Boit, A., Sakschewski, B., Boysen, L., Cano-Crespo, A., Clement, J., Garcia-Alaniz, N., et al. (2016). Large-scale impact of climate change vs. land-use change on future biome shifts in Latin America. *Global Change Biology*, *22*(11), 3689–3701. https://doi.org/10.1111/gcb.13355

Davies-Barnard, T., Valdes, P. J., Singarayer, J. S., Wiltshire, A. J., & Jones, C. D. (2015). Quantifying the relative importance of land cover change from climate and land use in the Representative Concentration Pathways. *Global Biogeochemical Cycles*, *29*, 842–853. https://doi.org/10.1002/2014GB004949

Davin, E. L., & de Noblet-Ducoudre, N. (2010). Climatic impact of global-scale deforestation: Radiative versus nonradiative processes. *Journal of Climate*, *23*(1), 97–112. https://doi.org/10.1175/2009JCLI3102.1

Devaraju, N., Bala, G., Caldeira, K., & Nemani, R. (2016). A model based investigation of the relative importance of CO_2-fertilization, climate warming, nitrogen deposition and land use change on the global terrestrial carbon uptake in the historical period. *Climate Dynamics*, *47*(1-2), 173–190. https://doi.org/10.1007/s00382-015-2830-8

Devaraju, N., Bala, G., & Nemani, R. (2015). Modelling the influence of land-use changes on biophysical and biochemical interactions at regional and global scales. *Plant Cell and Environment*, *38*(9), 1931–1946. https://doi.org/10.1111/pce.12488

Doelman, J. C., Stehfest, E., Tabeau, A., Van Meijl, H., Lassaletta, L., Gernaat, D. E. H. J., et al. (2018). Exploring SSP land-use dynamics using the IMAGE model: Regional and gridded scenarios of land-use change and land-based climate change mitigation. *Global Environmental Change*, *48*, 119–135. https://doi.org/10.1016/j.gloenvcha.2017.11.014

Dufresne, J. L., Foujols, M. A., Denvil, S., Caubel, A., Marti, O., Aumont, O., et al. (2013). Climate change projections using the IPSL-CM5 Earth System Model: From CMIP3 to CMIP5. *Climate Dynamics*, *40*(9-10), 2123–2165. https://doi.org/10.1007/s00382-012-1636-1

Duveiller, G., Forzieri, G., Robertson, E., Li, W., Georgievski, G., Lawrence, P., et al. (2018). Biophysics and vegetation cover change: A process-based evaluation framework for confronting land surface models with satellite observations. *Earth System Science Data*, *10*(3), 1265–1279. https://doi.org/10.5194/essd-10-1265-2018

Duveiller, G., Hooker, J., & Cescatti, A. (2018). A dataset mapping the potential biophysical effects of vegetation cover change. *Scientific Data*, *5*(1). https://doi.org/10.1038/Sdata.2018.14

Ellis, E. C., & Ramankutty, N. (2008). Putting people in the map: Anthropogenic biomes of the world. *Frontiers in Ecology and the Environment*, *6*(8), 439–447. https://doi.org/10.1890/070062

Ellison, D., Futter, M. N., & Bishop, K. (2012). On the forest cover-water yield debate: From demand- to supply-side thinking. *Global Change Biology*, *18*(3), 806–820. https://doi.org/10.1111/j.1365-2486.2011.02589.x

Field, C. B., Jackson, R. B., & Mooney, H. A. (1995). Stomatal responses to increased CO_2—Implications from the plant to the global-scale. *Plant Cell and Environment*, *18*(10), 1214–1225. https://doi.org/10.1111/j.1365-3040.1995.tb00630.x

Food and Agriculture Organization (1991), The digitized soil map of the world (Release 1.0). 67/1.

Food and Agriculture Organization (2012), Harmonized world soil database (version 1.2).

Friend, A. D., Lucht, W., Rademacher, T. T., Keribin, R., Betts, R., Cadule, P., et al. (2014). Carbon residence time dominates uncertainty in terrestrial vegetation responses to future climate and atmospheric CO_2. *Proceedings of the National Academy of Sciences of the United States of America*, *111*(9), 3280–3285. https://doi.org/10.1073/pnas.1222477110

Fujimori, S., Hasegawa, T., Masui, T., Takahashi, K., Herran, D. S., Dai, H. C., et al. (2017). SSP3: AIM implementation of shared socioeconomic pathways. *Global Environmental Change-Human and Policy Dimensions*, *42*, 268–283. https://doi.org/10.1016/j.gloenvcha.2016.06.009

Fuss, S., Lamb, W. F., Callaghan, M. W., Hilaire, J., Creutzig, F., Amann, T., et al. (2018). Negative emissions—Part 2: Costs, potentials and side effects. *Environmental Research Letters*, *13*(6). https://doi.org/10.1088/1748-9326/Aabf9f

Gedney, N., Cox, P. M., Betts, R. A., Boucher, O., Huntingford, C., & Stott, P. A. (2006). Detection of a direct carbon dioxide effect in continental river runoff records. *Nature*, *439*(7078), 835–838. https://doi.org/10.1038/nature04504

Gerten, D., Rost, S., Von Bloh, W., & Lucht, W. (2008). Causes of change in 20th century global river discharge. *Geophysical Research Letters*, *35*, L20405. https://doi.org/10.1029/2008gl035258

Goudriaan, J., & Van Laar, H. H. (1994). *Modelling potential crop growth processes: Textbook with exercises*. Dordrecht: Kluwer Academic Publishers. https://doi.org/10.1007/978-94-011-0750-1

Guo, L. B., & Gifford, R. M. (2002). Soil carbon stocks and land use change: A meta analysis. *Global Change Biology*, *8*(4), 345–360. https://doi.org/10.1046/j.1354-1013.2002.00486.x

Hansis, E., Davis, S. J., & Pongratz, J. (2015). Relevance of methodological choices for accounting of land use change carbon fluxes. *Global Biogeochemical Cycles*, *29*, 1230–1246. https://doi.org/10.1002/2014GB004997

Haverd, V., Cuntz, M., Nieradzik, L. P., & Harman, I. N. (2016). Improved representations of coupled soil-canopy processes in the CABLE land surface model (Subversion revision 3432). *Geoscientific Model Development*, *9*(9), 3111–3122. https://doi.org/10.5194/gmd-9-3111-2016

Haverd, V., Smith, B., Cook, G. D., Briggs, P. R., Nieradzik, L., Roxburgh, S. H., et al. (2013). A stand-alone tree demography and landscape structure module for Earth system models. *Geophysical Research Letters*, *40*, 5234–5239. https://doi.org/10.1002/grl.50972

Haverd, V., Smith, B., Nieradzik, L., Briggs, P. R., Woodgate, W., Trudinger, C. M., et al. (2018). A new version of the CABLE land surface model (Subversion revision r4601) incorporating land use and land cover change, woody vegetation demography, and a novel optimisation-based approach to plant coordination of photosynthesis. *Geoscientific Model Development*, *11*(7), 2995–3026. https://doi.org/10.5194/gmd-11-2995-2018

Haverd, V., Smith, B., Nieradzik, L. P., & Briggs, P. R. (2014). A stand-alone tree demography and landscape structure module for Earth system models: Integration with inventory data from temperate and boreal forests. *Biogeosciences*, *11*(15), 4039–4055. https://doi.org/10.5194/bg-11-4039-2014

He, T., Liang, S. L., & Song, D. X. (2014). Analysis of global land surface albedo climatology and spatial-temporal variation during 1981–2010 from multiple satellite products. *Journal of Geophysical Research: Atmospheres*, *119*, 10,281–10,298. https://doi.org/10.1002/2014JD021667

He, Y. J., Trumbore, S. E., Torn, M. S., Harden, J. W., Vaughn, L. J. S., Allison, S. D., & Randerson, J. T. (2016). Radiocarbon constraints imply reduced carbon uptake by soils during the 21st century. *Science*, *353*(6306), 1419–1424. https://doi.org/10.1126/science.aad4273

Heck, V., Gerten, D., Lucht, W., & Popp, A. (2018). Biomass-based negative emissions difficult to reconcile with planetary boundaries. *Nature Climate Change*, *8*(2), 151–155. https://doi.org/10.1038/s41558-017-0064-y

Hempel, S., Frieler, K., Warszawski, L., Schewe, J., & Piontek, F. (2013). A trend-preserving bias correction—The ISI-MIP approach. *Earth System Dynamics*, *4*(2), 219–236. https://doi.org/10.5194/esd-4-219-2013

Hurtt, G. C., Chini, L. P., Frolking, S., Betts, R. A., Feddema, J., Fischer, G., et al. (2011). Harmonization of land-use scenarios for the period 1500-2100: 600 years of global gridded annual land-use transitions, wood harvest, and resulting secondary lands. *Climatic Change*, *109*(1-2), 117–161. https://doi.org/10.1007/s10584-011-0153-2

Klein Goldewijk, K., Beusen, A., Doelman, J., & Stehfest, E. (2017). Anthropogenic land use estimates for the Holocene—HYDE 3.2. *Earth System Science Data*, *9*, 927–953. https://doi.org/10.5194/essd-9-927-2017

Kooperman, G. J., Fowler, M. D., Hoffman, F. M., Koven, C. D., Lindsay, K., Pritchard, M. S., et al. (2018). Plant-physiological responses to rising CO_2 modify simulated daily runoff intensity with implications for global-scale flood risk assessment. *Geophysical Research Letters*, *45*(22), 12,457–12,466. https://doi.org/10.1029/2018GL079901

Kowalczyk, E. A., Stevens, L., Law, R. M., Dix, M., Wang, Y. P., Harman, I. N., et al. (2013). The land surface model component of ACCESS: Description and impact on the simulated surface climatology. *Australian Meteorological and Oceanographic Journal*, *63*, 65–82. https://doi.org/10.22499/2.6301.005

Krause, A., Bayer, A. D., Pugh, T. A. M., Doelman, J. C., Humpenöder, F., Anthoni, P., et al. (2017). Global consequences of afforestation and bioenergy cultivation on ecosystem service indicators. *Biogeosciences*, *14*, 1–42. https://doi.org/10.5194/bg-2017-160

Krause, A., Pugh, T. A. M., Bayer, A. D., Lindeskog, M., & Arneth, A. (2016). Impacts of land-use history on the recovery of ecosystems after agricultural abandonment. *Earth System Dynamics*, *7*(3), 745–766. https://doi.org/10.5194/esd-7-745-2016

Kriegler, E., Bauer, N., Popp, A., Humpenoder, F., Leimbach, M., Strefler, J., et al. (2017). Fossil-fueled development (SSP5): An energy and resource intensive scenario for the 21st century. *Global Environmental Change-Human and Policy Dimensions*, *42*, 297–315. https://doi.org/10.1016/j.gloenvcha.2016.05.015

Le Quere, C., Andrew, R. M., Friedlingstein, P., Sitch, S., Pongratz, J., Manning, A. C., et al. (2018). Global carbon budget 2017. *Earth System Science Data*, *10*(1), 405–448. https://doi.org/10.5194/essd-10-405-2018

Levy, P. E., Cannell, M. G. R., & Friend, A. D. (2004). Modelling the impact of future changes in climate, CO_2 concentration and land use on natural ecosystems and the terrestrial carbon sink. *Global Environmental Change-Human and Policy Dimensions*, *14*(1), 21–30. https://doi.org/10.1016/j.gloenvcha.2003.10.005

Li, Q. P., Ma, M. G., Wu, X. D., & Yang, H. (2018). Snow cover and vegetation-induced decrease in global albedo from 2002 to 2016. *Journal of Geophysical Research: Atmospheres*, *123*(1), 124–138. https://doi.org/10.1002/2017JD027010

Li, W., Ciais, P., Peng, S. S., Yue, C., Wang, Y. L., Thurner, M., et al. (2017). Land-use and land-cover change carbon emissions between 1901 and 2012 constrained by biomass observations. *Biogeosciences*, *14*(22), 5053–5067. https://doi.org/10.5194/bg-14-5053-2017

Li, Y., Wang, T., Zeng, Z. Z., Peng, S. S., Lian, X., & Piao, S. L. (2016). Evaluating biases in simulated land surface albedo from CMIP5 global climate models. *Journal of Geophysical Research: Atmospheres*, *121*, 6178–6190. https://doi.org/10.1002/2016JD024774

Li, Y., Zhao, M. S., Motesharrei, S., Mu, Q. Z., Kalnay, E., & Li, S. C. (2015). Local cooling and warming effects of forests based on satellite observations. *Nature Communications*, *6*(1), 6603. https://doi.org/10.1038/Ncomms7603

Lindeskog, M., Arneth, A., Bondeau, A., Waha, K., Seaquist, J., Olin, S., & Smith, B. (2013). Implications of accounting for land use in simulations of ecosystem carbon cycling in Africa. *Earth System Dynamics*, *4*(2), 385–407. https://doi.org/10.5194/esd-4-385-2013

Loranty, M. M., Berner, L. T., Goetz, S. J., Jin, Y. F., & Randerson, J. T. (2014). Vegetation controls on northern high latitude snow-albedo feedback: Observations and CMIP5 model simulations. *Global Change Biology*, *20*(2), 594–606. https://doi.org/10.1111/gcb.12391

Mao, J. F., Fu, W. T., Shi, X. Y., Ricciuto, D. M., Fisher, J. B., Dickinson, R. E., et al. (2015). Disentangling climatic and anthropogenic controls on global terrestrial evapotranspiration trends. *Environmental Research Letters*, *10*(9). https://doi.org/10.1088/1748-9326/10/9/094008

McGuire, A. D., Sitch, S., Clein, J. S., Dargaville, R., Esser, G., Foley, J., et al. (2001). Carbon balance of the terrestrial biosphere in the twentieth century: Analyses of CO_2, climate and land use effects with four process-based ecosystem models. *Global Biogeochemical Cycles*, *15*(1), 183–206. https://doi.org/10.1029/2000gb001298

Müller, C., Eickhout, B., Zaehle, S., Bondeau, A., Cramer, W., & Lucht, W. (2007). Effects of changes in CO_2, climate, and land use on the carbon balance of the land biosphere during the 21st century. *Journal of Geophysical Research-Biogeosciences*, *112*(G2). https://doi.org/10.1029/2006jg000388

Olin, S., Schurgers, G., Lindeskog, M., Warlind, D., Smith, B., Bodin, P., et al. (2015). Modelling the response of yields and tissue C: N to changes in atmospheric CO_2 and N management in the main wheat regions of western Europe. *Biogeosciences*, *12*(8), 2489–2515. https://doi.org/10.5194/bg-12-2489-2015

Ostberg, S., Boysen, L. R., Schaphoff, S., Lucht, W., & Gerten, D. (2018). The biosphere under potential Paris outcomes. *Earths Future*, *6*(1), 23–39. https://doi.org/10.1002/2017EF000628

Ostberg, S., Schaphoff, S., Lucht, W., & Gerten, D. (2015). Three centuries of dual pressure from land use and climate change on the biosphere. *Environmental Research Letters*, *10*(4). https://doi.org/10.1088/1748-9326/10/4/044011

Pan, S. F., Tian, H. Q., Dangal, S. R. S., Yang, Q. C., Yang, J., Lu, C. Q., et al. (2015). Responses of global terrestrial evapotranspiration to climate change and increasing atmospheric CO_2 in the 21st century. *Earths Future*, *3*(1), 15–35. https://doi.org/10.1002/2014EF000263

Parton, W. J., Hanson, P. J., Swanston, C., Torn, M., Trumbore, S. E., Riley, W., & Kelly, R. (2010). ForCent model development and testing using the Enriched Background Isotope. *Study experiment. Journal of Geophysical Research-Biogeosciences*, *115*(G4). https://doi.org/10.1029/2009jg001193

Parton, W. J., Scurlock, J. M. O., Ojima, D. S., Gilmanov, T. G., Scholes, R. J., Schimel, D. S., et al. (1993). Observations and modeling of biomass and soil organic-matter dynamics for the grassland biome worldwide. *Global Biogeochemical Cycles*, *7*(4), 785–809. https://doi.org/10.1029/93gb02042

Piao, S. L., Friedlingstein, P., Ciais, P., de Noblet-Ducoudre, N., Labat, D., & Zaehle, S. (2007). Changes in climate and land use have a larger direct impact than rising CO_2 on global river runoff trends. *Proceedings of the National Academy of Sciences of the United States of America*, *104*, 15242–15247. https://doi.org/10.1073/pnas.0707213104

Popp, A., Calvin, K., Fujimori, S., Havlik, P., Humpenoder, F., Stehfest, E., et al. (2017). Land-use futures in the shared socio-economic pathways. *Global Environmental Change-Human and Policy Dimensions*, *42*, 331–345. https://doi.org/10.1016/j.gloenvcha.2016.10.002

Porporato, A., Laio, F., Ridolfi, L., & Rodriguez-Iturbe, I. (2001). Plants in water-controlled ecosystems: Active role in hydrologic processes and response to water stress—III. Vegetation water stress. *Advances in Water Resources*, *24*(7), 725–744. https://doi.org/10.1016/S0309-1708(01)00006-9

Pugh, T. A. M., Arneth, A., Olin, S., Ahlström, A., Bayer, A. D., Klein Goldewijk, K., et al. (2015). Simulated carbon emissions from land use change are substantially enhanced by accounting for agricultural management. *Environmental Research Letters*, *10*(12). https://doi.org/10.1088/1748-9326/10/12/124008

Qu, X., & Hall, A. (2014). On the persistent spread in snow-albedo feedback. *Climate Dynamics*, *42*(1-2), 69–81. https://doi.org/10.1007/s00382-013-1774-0

Quesada, B., Arneth, A., & de Noblet-Ducoudre, N. (2017). Atmospheric, radiative, and hydrologic effects of future land use and land cover changes: A global and multimodel climate picture. *Journal of Geophysical Research: Atmospheres*, *122*, 5113–5131. https://doi.org/10.1002/2016JD025448

Quesada, B., Arneth, A., Robertson, E., & de Noblet-Ducoudre, N. (2018). Potential strong contribution of future anthropogenic land-use and land-cover change to the terrestrial carbon cycle. *Environmental Research Letters*, *13*(6). https://doi.org/10.1088/1748-9326/Aac4c3

Roesch, A. (2006). Evaluation of surface albedo and snow cover in AR4 coupled climate models. *Journal of Geophysical Research-Atmospheres*, *111*(D15). https://doi.org/10.1029/2005jd006473

Seidl, R., Thom, D., Kautz, M., Martin-Benito, D., Peltoniemi, M., Vacchiano, G., et al. (2017). Forest disturbances under climate change. *Nature Climate Change*, *7*(6), 395–402. https://doi.org/10.1038/Nclimate3303

Shi, X. Y., Mao, J. F., Thornton, P. E., Hoffman, F. M., & Post, W. M. (2011). The impact of climate, CO_2, nitrogen deposition and land use change on simulated contemporary global river flow. *Geophysical Research Letters*, *38*, L08704. https://doi.org/10.1029/2011gl046773

Sitch, S., Smith, B., Prentice, I. C., Arneth, A., Bondeau, A., Cramer, W., et al. (2003). Evaluation of ecosystem dynamics, plant geography and terrestrial carbon cycling in the LPJ dynamic global vegetation model. *Global Change Biology*, *9*(2), 161–185. https://doi.org/10.1046/j.1365-2486.2003.00569.x

Smith, B., Warlind, D., Arneth, A., Hickler, T., Leadley, P., Siltberg, J., & Zaehle, S. (2014). Implications of incorporating N cycling and N limitations on primary production in an individual-based dynamic vegetation model. *Biogeosciences*, *11*(7), 2027–2054. https://doi.org/10.5194/bg-11-2027-2014

Tao, B., Tian, H. Q., Ren, W., Yang, J., Yang, Q. C., He, R. Y., et al. (2014). Increasing Mississippi River discharge throughout the 21st century influenced by changes in climate, land use, and atmospheric CO_2. *Geophysical Research Letters*, *41*, 4978–4986. https://doi.org/10.1002/2014GL060361

Thackeray, C. W., Qu, X., & Hall, A. (2018). Why do models produce spread in snow albedo feedback? *Geophysical Research Letters*, *45*(12), 6223–6231. https://doi.org/10.1029/2018GL078493

Tharammal, T., Bala, G., Narayanappa, D., & Nemani, R. (2018). Potential roles of CO_2 fertilization, nitrogen deposition, climate change, and land use and land cover change on the global terrestrial carbon uptake in the twenty-first century. *Climate Dynamics*, *52*(7-8), 4393–4406. https://doi.org/10.1007/s00382-018-4388-8

van Vuuren, D. P., Stehfest, E., Gernaat, D. E. H. J., Doelman, J. C., van den Berg, M., Harmsen, M., et al. (2017). Energy, land-use and greenhouse gas emissions trajectories under a green growth paradigm. *Global Environmental Change 42*, 237–250.

Wang, A. H., Xu, L. L., & Kong, X. H. (2018). Assessments of the Northern Hemisphere snow cover response to 1.5 and 2.0 degrees C warming. *Earth System Dynamics*, *9*(2), 865–877. https://doi.org/10.5194/esd-9-865-2018

Wang, Y. P., Kowalczyk, E., Leuning, R., Abramowitz, G., Raupach, M. R., Pak, B., et al. (2011). Diagnosing errors in a land surface model (CABLE) in the time and frequency domains. *Journal of Geophysical Research-Biogeosciences*, *116*(G1). https://doi.org/10.1029/2010jg001385

Wang, Y. P., Law, R. M., & Pak, B. (2010). A global model of carbon, nitrogen and phosphorus cycles for the terrestrial biosphere. *Biogeosciences*, *7*(7), 2261–2282. https://doi.org/10.5194/bg-7-2261-2010

Wang, Z., & Zeng, X. B. (2010). Evaluation of snow albedo in land models for weather and climate studies. *Journal of Applied Meteorology and Climatology*, *49*(3), 363–380. https://doi.org/10.1175/2009JAMC2134.1

Warlind, D., Smith, B., Hickler, T., & Arneth, A. (2014). Nitrogen feedbacks increase future terrestrial ecosystem carbon uptake in an individual-based dynamic vegetation model. *Biogeosciences*, *11*(21), 6131–6146. https://doi.org/10.5194/bg-11-6131-2014

Warszawski, L., Frieler, K., Huber, V., Piontek, F., Serdeczny, O., & Schewe, J. (2014). The Inter-Sectoral Impact Model Intercomparison Project (ISI-MIP): Project framework. *Proceedings of the National Academy of Sciences of the United States of America*, *111*, 3228–3232. https://doi.org/10.1073/pnas.1312330110

Xia, J. Y., Luo, Y. Q., Wang, Y. P., Weng, E. S., & Hararuk, O. (2012). A semi-analytical solution to accelerate spin-up of a coupled carbon and nitrogen land model to steady state. *Geoscientific Model Development*, *5*(5), 1259–1271. https://doi.org/10.5194/gmd-5-1259-2012

Zaehle, S., Bondeau, A., Carter, T. R., Cramer, W., Erhard, M., Prentice, I. C., et al. (2007). Projected changes in terrestrial carbon storage in Europe under climate and land-use change, 1990-2100. *Ecosystems*, *10*(3), 380–401. https://doi.org/10.1007/s10021-007-9028-9

Zhang, K., Castanho, A. D. D., Galbraith, D. R., Moghim, S., Levine, N. M., Bras, R. L., et al. (2015). The fate of Amazonian ecosystems over the coming century arising from changes in climate, atmospheric CO_2, and land use. *Global Change Biology*, *21*(7), 2569–2587. https://doi.org/10.1111/gcb.12903

Zhu, Z. C., Piao, S. L., Myneni, R. B., Huang, M. T., Zeng, Z. Z., Canadell, J. G., et al. (2016). Greening of the Earth and its drivers. *Nature Climate Change*, *6*(8), 791–795. https://doi.org/10.1038/Nclimate3004